arXiv:2608.04335v1 [stat.ME] 5 Aug 2026

Bivariate Prior Specification for Bayesian Decision-Making in Early-Phase Clinical Trials

Chengyuan Yang[1,*] and Evan Kwiatkowski[1]

[1]Department of Biostatistics and Data Science,

University of Texas Health Science Center at Houston, Houston, TX, USA

[*]Chengyuan.Yang@uth.tmc.edu

August 6, 2026

Abstract

Bayesian Go/No-Go decisions with co-primary endpoints require specifying prior distributions under the Normal-Inverse-Wishart framework; however guidance on how prior hyperparameters influence trial decisions remains limited. We propose a calibrated prior specification framework for bivariate Go/No-Go decisions. Skeptical and enthusiastic priors are calibrated so that each assigns a target probability to a clinically relevant decision region. We prove that for any prior precision $\kappa > 0$, a unique scale parameter λ_0 achieves the target calibration. Operating characteristics are evaluated across different κ via simulation and applied to a phase 3 telitacicept lupus trial.The simulation result indicates κ is the primary driver of prior discrimination. At $\kappa = 1$, the go rate difference between priors was 0.07; at $\kappa = 10$ it reached 0.56, with false positive rates below 0.01. Operating characteristics were robust to the degrees of freedom parameter ν_0 and prior correlation

ρ_0, supporting a default of $\nu_0 = 2$. In the lupus application, prior sensitivity was negligible at $\kappa = 1$ but at $\kappa = 10$ the enthusiastic go rate was three times the skeptical rate at small sample sizes. The framework reduces prior specification to two choices: the prior center and the prior precision κ. The identification of κ as the dominant parameter, together with the cautious choice of κ before the trial, motivates adaptive approaches to prior precision.

Keywords:

1 Introduction

Traditional clinical trial designs frequently rely on a single primary endpoint, such as a binary outcome (e.g., Objective Response Rates) or a continuous measure (e.g., survival time). The primary outcome could determine whether a trial proceeds to the next phase by evaluating treatment efficacy and safety. At the end of early phase studies, Go/No-Go (GNG) decisions are commonly informed by proof of concept evaluations, which are specifically designed to assess whether an investigational treatment shows sufficient promise to warrant progression[1]. These evaluations serve as critical decision points to determine whether a candidate should advance to later stage development. However, relying on a single endpoint often overlooks the complexity and heterogeneity of clinical outcomes, and may introduce bias in trial decision making[2]. For instance, endpoints such as time-to-event (TTE), Objective Response Rate (ORR), overall survival (OS), and progression-free survival (PFS), are widely used as the outcome measure in oncology trials to test patient's response to the drug [3]. While each provides clear and interpretable measures of treatment effect, simply relying on single endpoint may fail to capture the complex nature of disease progression or patient response. In practice, multiple endpoints often coexist and may provide complementary evidence, such as combining PFS and ORR when OS data are not yet mature, or using multiple outcomes measured at different stages with interim analyses. The growing complexity of clinical trials has highlighted the importance of addressing multiplicity when multiple endpoints are considered[4]; this issue has become a critical component of the drug development process, which requires thorough consideration and rigorous evaluation to meet regular standards, such as FDA approval criteria[5].

The use of co-primary endpoints has motivated substantial methodological development. Many trial designs have been proposed to jointly model correlated outcomes, including Bayesian copula-based approaches[6, 7, 8]. Beyond copula-based methods, there are methods that are tailored to specific endpoint types to address co-primary endpoints. Cho et al. proposed

a Bayesian design on a cure rate model that incorporated both TTE and PFS endpoints to evaluate cure status, using a bivariate copula with Cholesky decomposition [9] to estimate correlations between endpoints[10]. Yang et al. applied a Bayesian model on multinomial distribution to model sequentially occurring co-primary endpoints [11]. While these advanced methods have strengthened inference for co-primary endpoints, they have mainly focused on model specification and estimation. Zhao et al. proposed BOP2-DC, a Bayesian optimal phase II design that incorporates both statistical significance and clinical relevance into GNG decisions for multiple endpoints[12]. However, like earlier approaches, BOP2-DC focuses on optimizing the decision rule structure rather than examining how prior specification on the mean and covariance parameters influences the resulting decision. The question of how prior assumptions affect GNG operating characteristics in the co-primary setting has received little attention, despite the fact that in small samples the prior can substantially influence the posterior probability on which the decision is based.

Prior assumptions are particularly consequential in early-phase trial designs, where Bayesian methods are attractive for their natural support of probability-based decision rules and their ability to accommodate small sample sizes. In practice, GNG decisions can be based on posterior probabilities exceeding a pre-defined threshold, for instance, the posterior probability of superiority. Under such designs, the prior distribution interacts directly with the decision rule to determine the trial outcome, yet existing methods for co-primary endpoints have not systematically examined how prior specification affects these operating characteristics.

A broadly applicable framework for co-primary endpoints is the multivariate normal hierarchical model, since many endpoints can be represented as latent Gaussian variables. Under this model, it is common to place an inverse-Wishart prior on the covariance matrix due to conjugacy. However, common prior choices for variance parameters are known to impose undesirable constraints. The inverse-gamma prior on scalar variances concentrates excessive probability mass near zero even under seemingly noninformative specifications [13]. In practice, it shrinks

the variance aggressively, even though it was meant to be vague. The inverse-Wishart prior on covariance matrices couples the variance and correlation components, limiting independent control over each other [13]. The scaled inverse-Wishart reparameterization [14] offers greater flexibility, but practical guidance on how prior choices affect GNG decisions remains limited, especially in the small-sample settings typical of early-phase trials.

In this work, we address this gap by conducting a systematic evaluation of prior specification for bivariate GNG decisions under the conjugate Normal-Inverse-Wishart framework. We propose a calibration function that links prior hyperparameters to a prespecified level of skepticism or enthusiasm about treatment benefit.

We then prove existence and uniqueness of the calibrated scale parameter, and identify the prior precision κ as the primary driver of prior influence on trial decisions. We apply this framework retrospectively to a phase 3 telitacicept trial for systemic lupus erythematosus. The remainder of this paper is organized as follows: Section 2 describes the proposed methods, Section 3 presents the simulation study, Section 4 presents the motivating example, and Section 5 concludes with a discussion.

2 Methods

2.1 Bivariate Normal-Inverse-Wishart Model

Assume each subject is randomly assigned to one of two arms, $k \in \{A, B\}$, with n_k subjects per arm. Let $\mathbf{Y}_{ki} = (Y_{ki1}, Y_{ki2})^\top$ denote the bivariate outcome for subject i in arm k, where

$$\mathbf{Y}_{ki} \sim \mathcal{N}(\boldsymbol{\mu}_k, \Sigma), \quad \boldsymbol{\mu}_k = \begin{pmatrix} \mu_{k1} \\ \mu_{k2} \end{pmatrix}, \quad \Sigma = \begin{pmatrix} \sigma_1^2 & \rho\sigma_1\sigma_2 \\ \rho\sigma_1\sigma_2 & \sigma_2^2 \end{pmatrix}, \tag{1}$$

and observations are independent across arms. We adopt a conjugate Normal-Inverse-Wishart (NIW) prior for the arm-specific means and the shared covariance matrix:

$$\boldsymbol{\mu}_k \mid \Sigma \sim \mathcal{N}\Big(\boldsymbol{\mu}_{k0},\ \tfrac{1}{\kappa}\,\Sigma\Big), \qquad \Sigma \sim \text{InvWishart}(\nu_0,\ \Lambda), \tag{2}$$

where $\boldsymbol{\mu}_{k0}$ is the prior mean for arm k, and $\kappa > 0$ is the prior precision, shared across both arms ($\kappa_A = \kappa_B \equiv \kappa$). Higher value of κ indicates stronger prior confidence[15]. The prior scale matrix is decomposed as $\Lambda = \lambda_0 \cdot \Lambda_0$, where

$$\Lambda_0 = \begin{pmatrix} 1 & \rho_0 \\ \rho_0 & 1 \end{pmatrix} \tag{3}$$

encodes the prior correlation structure, and $\lambda_0 > 0$ is a scalar that controls the magnitude of the prior variance. This decomposition allows λ_0 to be tuned independently of the correlation structure.

Under this prior, the marginal distribution of the treatment effect $\boldsymbol{\delta} = \boldsymbol{\mu}_A - \boldsymbol{\mu}_B$ follows a bivariate t-distribution:

$$\boldsymbol{\delta} \sim t_{\nu_0+1-d}\Big(\boldsymbol{\delta}_0,\ \tfrac{2\lambda_0}{\kappa(\nu_0+1-d)}\,\Lambda_0\Big), \tag{4}$$

where $\boldsymbol{\delta}_0 = \boldsymbol{\mu}_{A0} - \boldsymbol{\mu}_{B0}$ and $d = 2$. The factor $2/\kappa$ in the scale reflects the equal-precision assumption across arms; the extension to unequal precisions replaces $\kappa/2$ with the harmonic mean $(\kappa_A^{-1} + \kappa_B^{-1})^{-1}$.

After observing data, the posterior distributions follow standard conjugate updating rules:

$$\boldsymbol{\mu}_k \mid \Sigma, \mathbf{Y} \sim \mathcal{N}\Big(\tfrac{\kappa\,\boldsymbol{\mu}_{k0} + n_k\,\bar{\mathbf{Y}}_k}{\kappa + n_k},\ \tfrac{1}{\kappa+n_k}\,\Sigma\Big), \tag{5}$$

$$\Sigma \mid \mathbf{Y}, \boldsymbol{\mu} \sim \text{InvWishart}(\nu_0 + n_A + n_B,\ \lambda_0\Lambda_0 + S_A + S_B), \tag{6}$$

where $\bar{\mathbf{Y}}_k = n_k^{-1} \sum_{i=1}^{n_k} \mathbf{Y}_{ki}$ is the sample mean for arm k, and S_k is the within-arm scatter matrix (definitions in Appendix 7.1). The posterior mean for each arm is a weighted average of the prior mean and the sample mean, with weight $\kappa/(\kappa + n_k)$ on the prior. Derivations are given in Appendix 7.1.

2.2 Decision rules

Based on the posterior distributions derived in Section 2.1, we consider a superiority decision rule comparing the mean efficacy between treatment arms A and B. The hypotheses are formulated as

$$H_0 : \boldsymbol{\mu}_A \leq \boldsymbol{\mu}_B \quad \text{versus} \quad H_1 : \boldsymbol{\mu}_A > \boldsymbol{\mu}_B, \tag{7}$$

where the inequalities are interpreted componentwise.

Let $\mathbf{Y}_A$ and $\mathbf{Y}_B$ denote the observed bivariate outcomes for the two arms. The posterior probability of superiority is then

$$\begin{aligned} P(\boldsymbol{\mu}_A > \boldsymbol{\mu}_B \mid \mathbf{Y}_A, \mathbf{Y}_B) &= P(\mu_{A1} > \mu_{B1},\, \mu_{A2} > \mu_{B2} \mid \mathbf{Y}_A, \mathbf{Y}_B) \\ &= \int_{-\infty}^{\infty}\int_{-\infty}^{\infty}\int_{\mu_{B2}}^{\infty}\int_{\mu_{B1}}^{\infty} f(\boldsymbol{\mu}_A, \boldsymbol{\mu}_B \mid \mathbf{Y}_A, \mathbf{Y}_B)\, d\mu_{A1}\, d\mu_{A2}\, d\mu_{B1}\, d\mu_{B2}. \end{aligned} \tag{8}$$

In practice, this is equivalent to $P(\boldsymbol{\delta} > \boldsymbol{\tau} \mid \text{data})$ where $\boldsymbol{\delta}$ follows the posterior marginal, and τ is the decision threshold vector.

Then, to induce a dichotomous decision on arm A is more efficacious than arm B, we use an indicator function with a threshold c:

$$\varphi(\mathbf{y}) = \begin{cases} 1 & \text{if } P(\boldsymbol{\delta} > \boldsymbol{\tau} \mid \text{data}) > c \\ 0 & \text{if } P(\boldsymbol{\delta} > \boldsymbol{\tau} \mid \text{data}) \leq c, \end{cases} \tag{9}$$

where 1 and 0 indicate the rejection and acceptance of the null hypothesis, respectively.

2.3 Enthusiastic and Skeptical Priors

We characterize prior informativeness through two contrasting specifications: the *skeptical prior* and the *enthusiastic prior*. Each is defined by its center $\boldsymbol{\delta}_0$ in the treatment-effect space and by the prior probability it assigns to a clinically relevant region before observing any data.

The skeptical prior is centered at or near the decision threshold $\boldsymbol{\tau}$, reflecting the belief that the treatment effect is unlikely to exceed the threshold for clinical relevance. Under this specification, the most prior mass concentrates near the threshold, and relatively little mass falls in the decision region $\{\boldsymbol{\delta} : \boldsymbol{\delta} > \boldsymbol{\tau}\}$ (Figure 1, right panel)

Conversely, the enthusiastic prior is centered at a positive effect above the threshold, reflecting optimism about treatment benefit. Under this specification, relatively little prior mass falls in the region of harm $\{\boldsymbol{\delta} : \boldsymbol{\delta} < \boldsymbol{\tau}\}$ (Figure 1, left panel).

To calibrate the scale parameter λ_0 for each prior, we define the calibration function

$$f(\lambda_0;\, \nu_0, \kappa, \boldsymbol{\delta}_0, \boldsymbol{\tau}) = P\big(\boldsymbol{\delta} \in \mathcal{R}^*\big), \tag{10}$$

where $\mathcal{R}^*$ denotes the relevant decision region and the probability is evaluated under the prior distribution Equation (4). In both cases, we solve for λ_0 such that $f(\lambda_0) = \alpha$, where α is a small target probability (e.g., 0.05). This ensures that both priors assign the same controlled amount of mass to their respective tail regions, providing a fair basis for comparison.

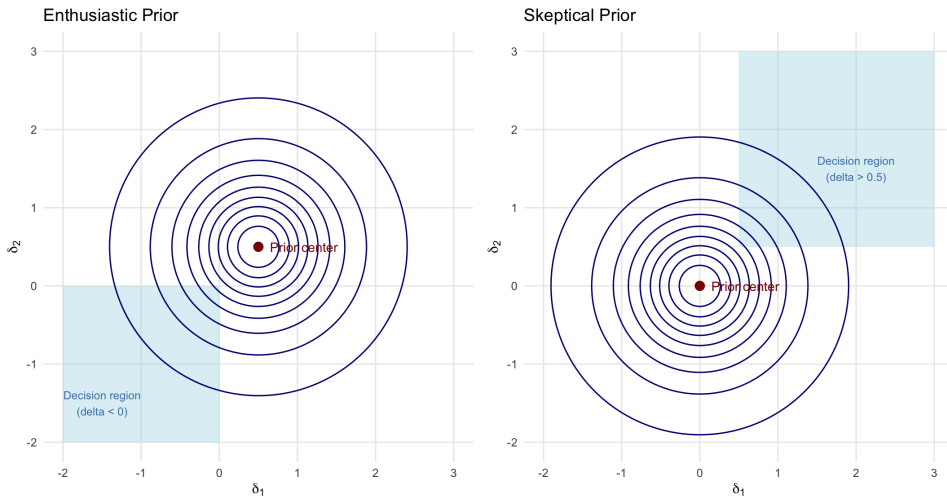

Figure 1: Illustration of the enthusiastic prior (left) centered at $\boldsymbol{\delta}_0 = (0.5, 0.5)$ and the skeptical prior (right) centered at $\boldsymbol{\delta}_0 = (0, 0)$, with $\nu_0 = 2$ and $\rho_0 = 0$. Contours show the bivariate t density of the marginal prior on $\boldsymbol{\delta}$. Shaded regions indicate the decision regions used for calibration. The scale parameter λ_0 is enlarged for visual clarity; calibrated values are reported in Supplementary Table S1.

2.4 Recommendation of default hyperparameters

The marginal prior on $\boldsymbol{\delta}$ in Equation (4) depends on three hyperparameters: the scale λ_0, the degrees of freedom ν_0, and the prior precision κ. To provide a principled default specification, we fix ν_0 and establish that for any $\kappa > 0$, a unique λ_0 can be calibrated to achieve a target level of prior skepticism or enthusiasm.

Proposition 1. *Let $f(\lambda_0;\ \nu_0, \kappa, \boldsymbol{\delta}_0, \boldsymbol{\tau})$ denote the calibration function* (10)*, defined as the prior probability that the treatment effect $\boldsymbol{\delta}$ falls in the decision region when the prior is centered at $\boldsymbol{\delta}_0$ with threshold $\boldsymbol{\tau}$. For the skeptical prior, $f = P(\boldsymbol{\delta} > \boldsymbol{\tau} \mid \boldsymbol{\delta}_0)$; for the enthusiastic prior, $f = P(\boldsymbol{\delta} < \boldsymbol{\tau} \mid \boldsymbol{\delta}_0)$.*

For fixed $\nu_0 > d - 1$, fixed $\kappa > 0$, and $\boldsymbol{\delta}_0 \neq \boldsymbol{\tau}$, $f(\lambda_0)$ is continuous and strictly monotone in

λ_0 on $(0, \infty)$ with boundary limits

$$\lim_{\lambda_0 \to 0} f(\lambda_0) \in \{0, 1\}, \qquad \lim_{\lambda_0 \to \infty} f(\lambda_0) = L,$$

where L is the orthant probability of the centered bivariate t distribution with correlation ρ_0 and $\nu_0 - d + 1$ degrees of freedom.

Consequently, for any target probability $\alpha \in (0, L)$, there exists a unique $\lambda_0^* > 0$ satisfying $f(\lambda_0^*) = \alpha$. This guarantee holds for every $\kappa > 0$: changing κ alters the scale of the prior on $\boldsymbol{\delta}$ through Equation (4)*, but the calibration function remains continuous and monotone in λ_0, so a unique recalibrated $\lambda_0^*(\kappa)$ exists at each κ.*

The proof is provided in Appendix 7.3.

This proposition ensures that the calibration framework is valid across the entire range of κ. For ν_0, we recommend the default $\nu_0 = \nu_{\min}$, the smallest integer satisfying $\nu_0 - d + 1 > 0$, which yields the heaviest-tailed and therefore least informative prior within the calibrated family. In the bivariate case ($d = 2$), this gives $\nu_0 = 2$. The simulation results in Supplementary table S2 confirm that operating characteristics are robust to ν_0, with correct prior ordering preserved across $\nu_0 \in \{2, 4, 10, 50\}$, supporting this default.

With ν_0 fixed, prior specification reduces to two interpretable choices: the prior center $\boldsymbol{\delta}_0$, which encodes the direction and magnitude of prior belief about treatment effect, and κ, controlling how strongly that belief influences the posterior.

3 Simulations

3.1 Operating characteristics

We simulated a two-arm trial with $n = 10$ subjects per arm. Two correlated endpoints were generated from a bivariate normal distribution with standard deviation 1 for both endpoints.

The true correlation was set at $\rho_{\text{true}} \in \{0, 0.6\}$, and the prior correlation at $\rho_0 \in \{0, 0.6\}$. True treatment effects were varied across four scenarios (Table 1); we report the null and both-effects scenarios in the main text.

For the skeptical prior, both arm-level prior means were set to be equal, giving $\boldsymbol{\delta}_0 = (0, 0)$. For the enthusiastic prior, the treatment arm prior mean was shifted so that $\boldsymbol{\delta}_0 = (0.5, 0.5)$. In both cases, λ_0 was calibrated with a fixed α, e.g. 0.05, in the target tail region. The degrees of freedom were fixed at the default $\nu_0 = 2$ throughout the main analysis. The prior precision was varied across $\kappa \in \{1, 5, 10\}$, with λ_0 recalibrated at each κ via Proposition 1 to maintain the target tail probability. For each configuration, 10,000 trials were simulated. A Go decision was declared if the posterior probability $P(\boldsymbol{\delta} > \boldsymbol{\tau} \mid \text{data})$ exceeded $c = 0.95$. The Go rate under the null scenario estimates the false positive rate, while under alternative scenarios it estimates power.

Scenario	Description of treatment arm	Mean structure (treatment A vs control B)
1	Null scenario	$\mu_{A1} - \mu_{B1} = \mu_{A2} - \mu_{B2} = 0$
2	Both endpoints have positive effects	$\mu_{A1} - \mu_{B1} = \mu_{A2} - \mu_{B2} > 0$
3	One endpoint effective, one nearly null	$\mu_{A1} - \mu_{B1} > 0, \quad \mu_{A2} - \mu_{B2} \approx 0$
4	Mixed magnitude positive effects	$\mu_{A1} - \mu_{B1} = 2(\mu_{A2} - \mu_{B2})$

Table 1: Data-generating scenarios for co-primary endpoints under two arms. Across all scenarios, treatment means $\mu_A \in \{0, 0.5, 1\}$, while control means μ_B are fixed as 0 to define the no effect.

3.2 Results

Table 2 reports the calibrated λ_0 values for each κ. The calibrated values confirm Proposition 1 that λ_0 increases with κ proportionally to compensate for the tighter prior scale. Figure 2 visualizes the calibration function for the skeptical prior across (κ, λ_0) with $\nu_0 = 2$ fixed. The contour lines trace the unique (κ, λ_0) pairs satisfying $f(\lambda_0) = \alpha$ for $\alpha = 0.05$ and $\alpha = 0.01$, illustrating the monotone relationship established in Proposition 1. Figure 2 shows that as $\lambda_0 \to$

∞, the calibration function converges to the orthant probability $L = 1/4 + \arcsin(\rho_0)/(2\pi)$, which equals 0.25 when $\rho_0 = 0$ and increases to approximately 0.35 when $\rho_0 = 0.6$(Lemma 3 in Appendix 7.3). By the symmetry of the calibration function, the enthusiastic prior produces identical λ_0 values at each κ, as shown in Figure S1.

Table 2: Prior specifications for the skeptical and enthusiastic priors. For each κ, λ_0 is calibrated via the calibration function (10) to achieve a target tail probability of $\alpha = 0.05$. All specifications use $\nu_0 = 2$ and $\rho_0 = 0$.

			Calibrated λ_0		
Prior	Center $\boldsymbol{\delta}_0$	Threshold $\boldsymbol{\tau}$	$\kappa = 1$	$\kappa = 5$	$\kappa = 10$
Skeptical	(0, 0)	(0.5, 0.5)	0.019	0.097	0.194
Enthusiastic	(0.5, 0.5)	(0, 0)	0.019	0.097	0.194

By the symmetry of the calibration function, both priors yield identical λ_0 at each κ. Target tail probability: $P(\boldsymbol{\delta} > \boldsymbol{\tau}) = 0.05$ for the skeptical prior; $P(\boldsymbol{\delta} < \boldsymbol{\tau}) = 0.05$ for the enthusiastic prior.

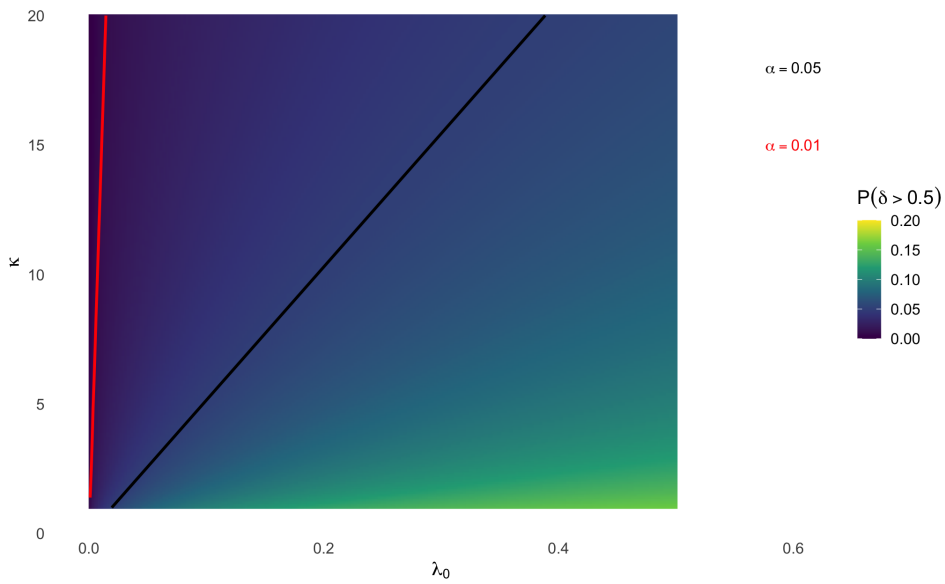

(a) $\rho_0 = 0$

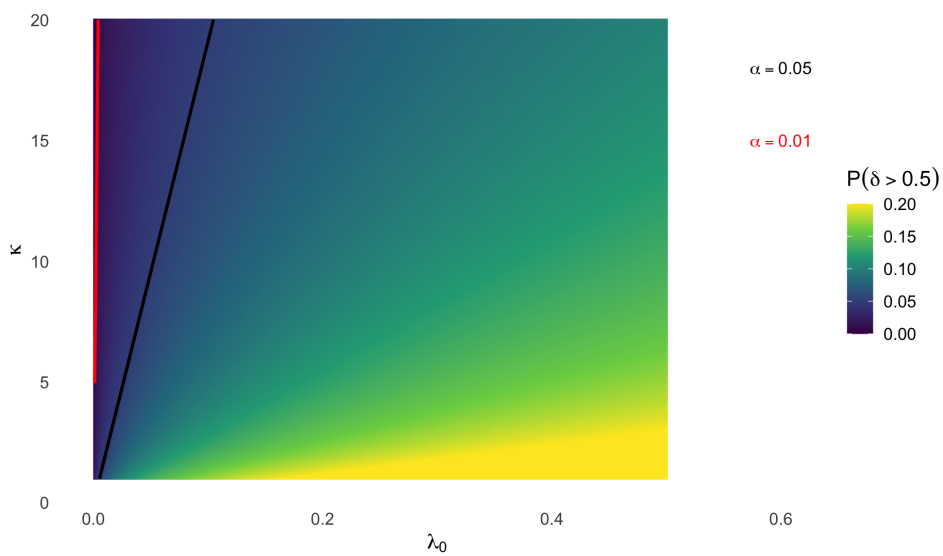

(b) $\rho_0 = 0.6$

Figure 2: Calibration function $P(\boldsymbol{\delta} > \boldsymbol{\tau})$ for the skeptical prior across (κ, λ_0) with $\nu_0 = 2$. Contour lines indicate $\alpha = 0.05$ (black) and $\alpha = 0.01$ (red). The contour lines trace the (κ, λ_0) pairs satisfying the calibration in Proposition 1.

Table 3 reports go rates for skeptical and enthusiastic priors across $\kappa \in \{1, 5, 10\}$, with ν_0 fixed at its default value of 2 and recalibrated λ_0 at each κ to maintain the 0.05 target tail probability. The results demonstrate that κ is the primary driver of prior distinction in this framework. Especially looking at the strong effect size case, at $\kappa = 1$, the difference between enthusiastic and skeptical go rates is only about 0.07. Increasing to $\kappa = 5$ raises this difference to 0.324, and at $\kappa = 10$ it reaches 0.57, where a skeptical prior yields a go rate of only 0.07 compared to 0.63 for the enthusiastic prior. Thus, although this recalibration maintains the same target tail probability across all κ values, it does not offset the direct effect of κ on the posterior mean weight $\kappa/(\kappa + n)$.

This amplification is explained by the posterior mean weight. A larger κ pulls the posterior mean more strongly toward the prior center, producing systematically higher Go rates for the enthusiastic prior and lower Go rates for the skeptical prior from the same observed data. Importantly, false positive rates remain controlled across all κ values, (less than 0.01 for the null scenario), confirming that increased prior discrimination does not come at the cost of inflated false positive rate.

Increasing sample size raises go rates substantially and reduces prior sensitivity. At $n = 50$ under the strong effect, go rates exceed 0.99 for both priors regardless of κ, indicating that the data dominate the posterior at this sample size. The κ effect is most pronounced at $n = 10$, where prior beliefs carry the greatest relative weight.

True endpoint correlation also increases go rates. Under $\rho_{\text{true}} = 0.6$, go rates are approximately 5 to 10 percentage points higher than under independence across all settings, reflecting the additional information gained from correlated endpoints. However, the prior correlation assumption ρ_0 has minimal impact. Results under $\rho_0 = 0.6$ (Supplementary Table S3) are similar to those under $\rho_0 = 0$, indicating that misspecification of the prior correlation does not affect operating characteristics. Importantly, false positive rates remain below 0.01 across all κ values and correlation structures, confirming that increased prior discrimination does not

inflate type I error.

Table 3: Go rates for skeptical and enthusiastic priors across $\kappa \in \{1, 5, 10\}$ and sample sizes, under the both-effects scenario, $\nu_0 = 2$, $c = 0.95$, 10,000 replications. For each κ, λ_0 is recalibrated to maintain the target tail probability of 0.05.

		$\rho_0 = 0,\ \rho_{\text{true}} = 0$			$\rho_0 = 0,\ \rho_{\text{true}} = 0.6$		
κ	Prior	Null	Moderate	Strong	Null	Moderate	Strong
$n = 10$ *per arm*							
1	Skeptical	0.0021	0.0658	0.4417	0.0122	0.1429	0.5269
	Enthusiastic	0.0027	0.0902	0.5097	0.0168	0.1750	0.5889
5	Skeptical	0.0004	0.0228	0.2263	0.0043	0.0659	0.3416
	Enthusiastic	0.0048	0.1158	0.5505	0.0229	0.2102	0.6245
10	Skeptical	0.0000	0.0035	0.0696	0.0013	0.0204	0.1598
	Enthusiastic	0.0085	0.1703	0.6321	0.0378	0.2857	0.6887
$n = 25$ *per arm*							
1	Skeptical	0.0017	0.2547	0.9265	0.0101	0.3562	0.9387
	Enthusiastic	0.0025	0.2869	0.9387	0.0125	0.3881	0.9505
5	Skeptical	0.0005	0.1925	0.8923	0.0069	0.2957	0.9144
	Enthusiastic	0.0039	0.3467	0.9553	0.0188	0.4474	0.9638
10	Skeptical	0.0002	0.1320	0.8445	0.0035	0.2291	0.8683
	Enthusiastic	0.0070	0.4405	0.9717	0.0317	0.5318	0.9745
$n = 50$ *per arm*							
1	Skeptical	0.0014	0.6114	0.9992	0.0099	0.6702	0.9994
	Enthusiastic	0.0016	0.6351	0.9995	0.0113	0.6914	0.9995
5	Skeptical	0.0012	0.5742	0.9986	0.0082	0.6364	0.9990
	Enthusiastic	0.0031	0.6954	0.9997	0.0164	0.7356	0.9995
10	Skeptical	0.0005	0.5313	0.9980	0.0064	0.5986	0.9980
	Enthusiastic	0.0054	0.7607	0.9997	0.0260	0.7902	0.9998

ρ_0: prior correlation in Λ_0; ρ_{true}: true correlation used to generate data. Null: $\boldsymbol{\delta} = (0, 0)$; Moderate : $\boldsymbol{\delta} = (0.5, 0.5)$; Strong: $\boldsymbol{\delta} = (1, 1)$.

4 Motivating example: the Telitacicept Lupus Trial

To illustrate the proposed Bayesian decision framework in a real clinical setting, we applied it retrospectively to a phase 3 trial of telitacicept for systemic lupus erythematosus [16]. The trial randomized 167 participants to the telitacicept arm and 168 to placebo. The primary endpoint was a binary SRI-4 composite responder rate at week 52, defined as a simultaneous reduction of at least 4 points from baseline in the SELENA-SLEDAI score, no new disease activity as measured by the BILAG index[17, 18], and no worsening in the Physician's Global Assessment (PGA) score[19]. The secondary endpoints included the continuous component measures of the SRI-4 assessed separately: the mean change from baseline in SELENA-SLEDAI score and the mean change from baseline in PGA score, both at week 52. For this application, we focus on two continuous secondary endpoints. Since the original trial reports treatment improvement as a negative change, we flipped the sign of all outcomes so that a positive change is consistent with the decision rule.

Data generation

The true treatment means on the flipped scale were taken directly from the paper: μ_T = (4.95, 0.79) for the telitacicept arm and μ_C = (1.00, 0.40) for the placebo arm, corresponding to SELENA-SLEDAI and PGA respectively. Since individual patient-level data were unavailable, the endpoint standard deviations were recovered from the reported Wald 95 confidence intervals using the estimation, yielding σ_T = (19.3, 0.69) and σ_C = (22.0, 0.51) for the treatment and placebo arms, respectively.

Post-treatment SELENA-SLEDAI scores were generated from a lognormal distribution to reflect the non-negative and right-skewed nature of the score. Specifically, baseline scores $X_0 \sim \text{LogNormal}(\mu_{0,\log}, \sigma^2_{0,\log})$ and post-treatment scores $X_1 \sim \text{LogNormal}(\mu_{1,\log}, \sigma^2_{1,\log})$ were generated independently, with the change score computed as $\Delta = -(X_1 - X_0)$ on the flipped

scale. Lognormal parameters were derived from:

$$\mu_{\log} = \log(E[X]) - \frac{\sigma^2_{\log}}{2}, \quad \sigma^2_{\log} = \log\left(1 + \frac{\mathrm{SD}^2}{E[X]^2}\right),$$

yielding $(\mu_{0,\log}, \sigma^2_{0,\log}) = (2.407, 0.070)$ for baseline and $(\mu_{1T,\log}, \sigma^2_{1T,\log}) = (0.755, 2.247)$ for the treatment arm post-treatment score. This approach improved the simulated SELENA-SLEDAI responder rate from 52% under normality to 77%, closer to the observed 70.1%. PGA changes were generated from a normal distribution. The analysis model assumed bivariate normality throughout, consistent with the NIW conjugate framework.

Correlation Estimation

Since this trial does not directly report the correlation between SELENA-SLEDAI and PGA score, we estimated the correlation based on the binary response and the marginal responder rate for each outcome individually. Assuming the BILAG component of SRI-4 is independent to SELENA-SLEDAI and PGA, the SRI-4 responder probability can be approximated as the joint probability $P(X_{\mathrm{SELENA}} \geq 4 \text{ and } X_{\mathrm{PGA}} \geq -0.3) = \Phi_2(-c_1, -c_2; \rho)$, where Φ_2 is the standard bivariate normal CDF with correlation ρ. The threshold $c_1 \approx -0.527$ was derived from the observed marginal SELENA-SLEDAI rate of 0.701, and $c_2 \approx -1.574$ was derivedd from the mean PGA change. Setting $\Phi_2(-c_1, -c_2; \rho) = 0.671$ and solving numerically via bisection, we obtain $\hat{\rho} = 0.239$.

Results

Table 4 reports go rates for the telitacicept lupus trial application across prior precision values $\kappa \in \{1, 5, 10\}$ and sample sizes $n \in \{20, 50, 80, 167\}$ per arm, with superiority threshold. Prior centers were matched to the SRI-4 clinical efficacy criteria. The skeptical prior was centered at $(4, 0.3)$, corresponding to the minimum clinically meaningful threshold, and the enthusiastic

prior at $(8, 0.6)$, representing a treatment effect twice the minimum threshold.

At the default prior precison $\kappa = 1$ per arm, go rates are very similar between enthusiastic prior and skeptical prior, at most 0.013 at $n = 20$ and drop to 0.005 at full sample size $n = 167$. This mirrors the general simulation finding that $\kappa = 1$ produces negligible prior sensitivity. At $\kappa = 5$, the enthusiastic prior yields a go rate of 0.165 at $n = 20$ compared to 0.087 for the skeptical prior, a difference of 0.078. At $\kappa = 10$ and $n = 20$, this gap widens to 0.189 with the enthusiastic go rate (0.282) roughly three times to the skeptical go rate (0.093). This shows that meaningful prior discrimination emerges in the lupus application only when κ is sufficiently large relative to the sample size, confirming κ as the primary driver of prior influence identified in the general simulation.

The interaction between κ and sample size is also apparent. At $n = 167$, even $\kappa = 10$ produces a modest difference of 0.038 between priors (0.652 versus 0.614), because the large sample size dilutes the prior's contribution to the posterior.

Table 4: Go rates for skeptical and enthusiastic priors under the telitacicept lupus trial application across prior precision values $\kappa \in \{1, 5, 10\}$ and sample sizes, $\nu_0 = 2$, $\rho_0 = 0$, $\rho_{\text{true}} = 0$, using control $\boldsymbol{\mu}_C = (1.00, 0.40)$, superiority threshold $\boldsymbol{\delta} > (0, 0)$, $c = 0.95$, 10,000 replications.

		Go Rate			
κ	Prior	$n = 20$	$n = 50$	$n = 80$	$n = 167$
1	Skeptical	0.0795	0.2492	0.3764	0.5843
	Enthusiastic	0.0924	0.2618	0.3849	0.5892
5	Skeptical	0.0874	0.2611	0.3947	0.5960
	Enthusiastic	0.1652	0.3224	0.4382	0.6170
10	Skeptical	0.0932	0.2853	0.4097	0.6135
	Enthusiastic	0.2820	0.4062	0.4927	0.6518

Skeptical prior centred at $(4,\ 0.3)$ with target probability 0.05 in the upper tail; enthusiastic prior centred at $(8,\ 0.6)$ with target probability 0.05 in the lower tail, corresponding to the SRI-4 minimum efficacy threshold and twice the threshold respectively. Data generated from a lognormal distribution for SELENA-SLEDAI and normal distribution for PGA. True treatment mean $\boldsymbol{\mu}_T = (4.95,\ 0.79)$.

5 Discussion

We have proposed a calibrated prior specification framework for bivariate Bayesian Go/No-Go decisions under the Normal–Inverse–Wishart model, and systematically examined how the hyperparameters λ_0, ν_0, and κ influence prior informativeness and posterior operating characteristics. The calibration function links prior hyperparameters to a prespecified clinical statement (e.g. a specified level of prior skepticism or enthusiasm about treatment benefit) through a linked pair (κ, λ_0). The prior precision κ controls how strongly prior beliefs influence the posterior through the weight on the prior mean, while λ_0 is recalibrated at each κ via Proposition 1 to preserve the target tail probability. The degrees of freedom parameter ν_0 governs the tail shape of the prior but, as confirmed by simulation, has minimal impact on operating characteristics, supporting choosing the default value of ν_0.

In contrast, the prior precision κ emerged as the primary driver of prior discrimination. Although λ_0 is recalibrated at each κ to maintain the target tail probability, this does not diminish the direct effect of κ on the posterior mean. At $\kappa = 1$ and $n = 10$ per arm, the prior contributes roughly 9% of the posterior mean, and the difference in go rates between priors was modest (0.068 under the strong effect). At $\kappa = 10$, the prior weight rises to 50%, and the go rate difference reaches 0.56, with false positive rates remaining below 0.01. This identifies κ as a clinically interpretable design parameter that directly governs how strongly prior beliefs influence the trial decision when sample sizes are small.

Regarding the role of correlation, the true endpoint correlation ρ_{true} meaningfully increased power, with go rates approximately 5 to 10 percentage points higher under $\rho_{\text{true}} = 0.6$ compared to independence across all configurations. In contrast, the prior correlation ρ_0 had negligible impact; the maximum absolute difference in go rates between $\rho_0 = 0$ and $\rho_0 = 0.6$ was 0.017. This asymmetry arises because ρ_0 enters the posterior only through the prior scale matrix $\Lambda = \lambda_0 \Lambda_0$, whose contribution to the posterior trace is bounded. It is negligible under the

default $\nu_0 = 2$, constraining λ_0 to be small (Appendix 7.2). This insensitivity has a practical advantage; the practitioner need not estimate or specify ρ_0 at the design stage, as any value in $(-1, 1)$ yields essentially identical operating characteristics.

The telitacicept lupus trial application validated these findings in a real clinical setting. At $\kappa = 1$, the difference in go rates between skeptical and enthusiastic priors was at most 0.013, consistent with the low signal-to-noise ratio of the SELENA-SLEDAI endpoint (SNR ≈ 0.20). Under these conditions, the likelihood dominates the posterior regardless of prior specification, and the go rate is driven primarily by sample size rather than prior choice. At $\kappa = 10$, however, meaningful differences appeared. The enthusiastic go rate at the total sample size of 40 was approximately three times the skeptical rate (0.282 versus 0.093). This difference disappeared with increasing sample size, falling to 0.038 at the total sample size of about 300, consistent with the theoretical prediction that larger samples dilute the prior's contribution. This motivating example thus demonstrates that the framework is sensitive to the interaction between κ, sample size, and the endpoint noise structure, and that prior precision matters most in the small-sample setting where Go/No-Go decisions are typically made.

This model has limitations within this model. First, the analysis model assumes bivariate normality throughout, while the motivating example endpoint was generate from a lognormal distribution to better match the non-negative observed responder rate. The impact of this mismatch between the data-generating mechanism and the assumed normal likelihood on posterior calibration deserves further study, particularly for endpoints with heavy skewness. Second, the prior scale matrix Λ_0 was specified with a unit diagonal, which treats both endpoints as operating on the same scale. In the lupus application, SELENA-SLEDAI has a standard deviation much higher than PGA, so the prior exerts differential influence across endpoints. Third, the correlation between endpoints was estimated indirectly from aggregate statistics under an independence assumption for the BILAG component of the SRI-4 composite, introducing uncertainty that was not propagated through the simulation.

In summary, the proposed framework provides a principled and interpretable approach to prior specification for bivariate Bayesian Go/No-Go decisions. The calibration function guarantees existence and uniqueness of the scale parameter for any target probability, and the default recommendation of $\nu_0 = 2$ simplifies prior parameters to the choice of κ and the prior center. The identification of κ as the primary driver of prior sensitivity, together with the practical difficulty of specifying the optimal κ before the trial, provides the central motivation for future work, where κ is treated as an adaptive parameter updated at interim to reflect the consistency between prior beliefs and accumulating data.

6 Software

All analyses were performed in R (version 4.4.0). Multivariate t distribution and probabilities were computed using the `mvtnorm` package [20].

References

[1] Sheldon H. Preskorn. The role of proof of concept (poc) studies in drug development using the evp-6124 poc study as an example. *Journal of Psychiatric Practice*, 20(1):59–60, January 2014.

[2] Charlie McLeod, Richard Norman, Edward Litton, Benjamin R Saville, Steve Webb, and Thomas L Snelling. Choosing primary endpoints for clinical trials of health care interventions. *Contemporary clinical trials communications*, 16:100486, 2019.

[3] Alejandro Delgado and Achuta K. Guddati. Clinical endpoints in oncology - a primer. *American Journal of Cancer Research*, 11(4):1121–1131, 2021.

[4] Gang Li, Monica Taljaard, Edwin R. Van den Heuvel, Mitchell A. Levine, Deborah J. Cook, George A. Wells, P. J. Devereaux, and Lehana Thabane. An introduction to multiplicity issues in clinical trials: the what, why, when and how. *International Journal of Epidemiology*, 46(2):746–755, 2017. PMID: 28025257.

[5] U.S.Food and Drug Administration. Multiple endpoints in clinical trials guidance for industry, 2022. Accessed: date-of-access.

[6] Roger B Nelsen. *An introduction to copulas*. Springer, 2006.

[7] Guosheng Yin. *Clinical trial design: Bayesian and frequentist adaptive methods*, volume 876. John Wiley & Sons, 2012.

[8] Kristen Cunanan and Joseph S Koopmeiners. Evaluating the performance of copula models in phase i-ii clinical trials under model misspecification. *BMC Medical Research Methodology*, 14(1):51, 2014.

[9] Nicholas J. Higham. *Analysis of the Cholesky decomposition of a semi-definite matrix*, pages 161–185. 1990.

[10] Matthew A. Psioda Seoyoon Cho and Joseph G. Ibrahim. Bayesian design of clinical trials with multiple time-to-event outcomes subject to functional cure. *Journal of Biopharmaceutical Statistics*, 0(0):1–12, 2025. PMID: 39865704.

[11] J. Yang, G. Li, D. Yang, J. Wu, J. Wang, X. Gao, and P. Liu. Seamless phase 2/3 design for trials with multiple co-primary endpoints using bayesian predictive power. *BMC Medical Research Methodology*, 24(1):12, Jan 2024.

[12] Yujie Zhao, Daniel Li, Rong Liu, and Ying Yuan. Bayesian optimal phase ii designs with dual-criterion decision making. *Pharmaceutical statistics*, 22(4):605–618, 2023.

[13] Andrew Gelman. Prior distributions for variance parameters in hierarchical models (comment on article by browne and draper). *Bayesian Analysis*, 1(3):515–534, September 2006.

[14] Andrew Gelman, John B Carlin, Hal S Stern, David B Dunson, Aki Vehtari, and Donald B Rubin. Bayesian data analysis third edition. *Chapman and Hall/CRC*, 2013.

[15] Yusuke Yamaguchi and Yifei Huang. *powerprior: Conjugate Power Priors for Bayesian Analysis of Normal Data*, 2025. R package version 1.0.0.

[16] Ronald F van Vollenhoven, Li Wang, Joan T Merrill, Yi Liu, Chunde Bao, Fen Li, Jiankang Hu, Chenghui Huang, Jianhong Zhao, Cibo Huang, et al. A phase 3 trial of telitacicept for systemic lupus erythematosus. *New England Journal of Medicine*, 393(15):1475–1485, 2025.

[17] DA Isenberg, A Rahman, EBILAG Allen, V Farewell, M Akil, IN Bruce, D D'cruz, B Griffiths, M Khamashta, P Maddison, et al. Bilag 2004. development and initial

validation of an updated version of the british isles lupus assessment group's disease activity index for patients with systemic lupus erythematosus. *Rheumatology*, 44(7):902–906, 2005.

[18] Chee-Seng Yee, Vernon Farewell, David A Isenberg, Bridget Griffiths, Lee-Suan Teh, Ian N Bruce, Yasmeen Ahmad, Anisur Rahman, Athiveeraramapandian Prabu, Mohammed Akil, et al. The bilag-2004 index is sensitive to change for assessment of sle disease activity. *Rheumatology*, 48(6):691–695, 2009.

[19] Michelle Petri, Mimi Y Kim, Kenneth C Kalunian, Jennifer Grossman, Bevra H Hahn, Lisa R Sammaritano, Michael Lockshin, Joan T Merrill, H Michael Belmont, Anca D Askanase, et al. Combined oral contraceptives in women with systemic lupus erythematosus. *New England Journal of Medicine*, 353(24):2550–2558, 2005.

[20] Alan Genz and Frank Bretz. *Computation of Multivariate Normal and t Probabilities*. Lecture Notes in Statistics. Springer-Verlag, Heidelberg, 2009.

[21] IG Abrahamson. Orthant probabilities for the quadrivariate normal distribution. *The Annals of Mathematical Statistics*, 35(4):1685–1703, 1964.

7 Supplementary Material

7.1 Derivation Proof

Marginal prior derivation. To prove equation 4, given that the pdf of inverse wishart distribution is approximate to:

$$p(\Sigma) = \frac{|\lambda_0\Lambda_0|^{\nu_0/2}|\Sigma|^{-(\nu_0+d+1)/2}\exp\Big[-\frac{1}{2}\mathrm{tr}\big(\lambda_0\Lambda_0\,\Sigma^{-1}\big)\Big]}{2^{\nu_0 * d/2}\Gamma(\nu_0/2)}, \quad (d = 2).$$

$$\begin{aligned}
p(\boldsymbol{\mu}_A) &= \int p(\boldsymbol{\mu}_A \mid \Sigma)\, p(\Sigma)\, d\Sigma \\
&\propto \int (2\pi)^{-\frac{1}{2}}\,|\Sigma|^{-\frac{1}{2}}\exp\Big(-\tfrac{\kappa}{2}(\boldsymbol{\mu}_A-\boldsymbol{\mu}_{A0})^\top\Sigma^{-1}(\boldsymbol{\mu}_A-\boldsymbol{\mu}_{A0})\Big) \times \frac{|\lambda_0\Lambda_0|^{\frac{\nu_0}{2}}\,|\Sigma|^{-\frac{\nu_0+d+1}{2}}\exp\big[-\frac{1}{2}\mathrm{tr}(\lambda_0\Lambda_0\Sigma^{-1})\big]}{2^{\frac{\nu_0 d}{2}}\,\Gamma(\frac{\nu_0}{2})} \\
&\propto \int |\Sigma|^{-\frac{\nu_0+d+2}{2}}\exp\Big(-\tfrac{1}{2}\mathrm{tr}\Big(\lambda_0\Lambda_0\Sigma^{-1}\Big) - \tfrac{\kappa}{2}(\boldsymbol{\mu}_A-\boldsymbol{\mu}_{A0})^\top\Sigma^{-1}(\boldsymbol{\mu}_A-\boldsymbol{\mu}_{A0})\Big)\, d\Sigma \\
&\propto \int |\Sigma|^{-\frac{\nu_0+d+2}{2}}\exp\Big(-\tfrac{1}{2}\mathrm{tr}\Big(\lambda_0\Lambda_0 + \kappa(\boldsymbol{\mu}_A-\boldsymbol{\mu}_{A0})(\boldsymbol{\mu}_A-\boldsymbol{\mu}_{A0})^\top\Big)\Sigma^{-1}\Big)\, d\Sigma
\end{aligned}$$

since the integrand is the kernel of $\mathrm{InvWishart}\big(\nu_0+1,\ \lambda_0\Lambda_0 + \kappa(\boldsymbol{\mu}_A-\boldsymbol{\mu}_{A0})(\boldsymbol{\mu}_A-\boldsymbol{\mu}_{A0})^\top\big)$,

$$\propto \frac{2^{\frac{(\nu_0+1)d}{2}}\,\Gamma\Big(\frac{\nu_0+1}{2}\Big)}{\Big|\lambda_0\Lambda_0 + \kappa(\boldsymbol{\mu}_A-\boldsymbol{\mu}_{A0})(\boldsymbol{\mu}_A-\boldsymbol{\mu}_{A0})^\top\Big|^{\frac{\nu_0+1}{2}}}.$$

Applying the matrix determinant lemma,

$$\Big|\lambda_0\Lambda_0 + \kappa(\boldsymbol{\mu}_A-\boldsymbol{\mu}_{A0})(\boldsymbol{\mu}_A-\boldsymbol{\mu}_{A0})^\top\Big| = |\lambda_0\Lambda_0|\left(1 + \tfrac{\kappa}{\lambda_0}(\boldsymbol{\mu}_A-\boldsymbol{\mu}_{A0})^\top(\Lambda_0)^{-1}(\boldsymbol{\mu}_A-\boldsymbol{\mu}_{A0})\right).$$

Then, multiplying the normalized constant, Therefore,

$$p(\boldsymbol{\mu}_A) = \frac{\Gamma\left(\frac{\nu_0+1}{2}\right)}{\Gamma\left(\frac{\nu_0}{2}\right)} \frac{1}{\left[1 + \frac{\kappa}{\lambda_0}(\boldsymbol{\mu}_A - \boldsymbol{\mu}_{A0})^\top (\Lambda_0)^{-1}(\boldsymbol{\mu}_A - \boldsymbol{\mu}_{A0})\right]^{\frac{\nu_0+1}{2}}}. \tag{11}$$

Up to the normalizing constant, this is the kernel of a multivariate t distribution:

$$\boldsymbol{\mu}_A \;\sim\; t_{\nu_0+1-d}\left(\boldsymbol{\mu}_{A0},\; \frac{\lambda_0}{\kappa(\nu_0+1-d)}\Lambda_0\right).$$

Similarly,

$$\boldsymbol{\mu}_B \;\sim\; t_{\nu_0+1-d}\left(\boldsymbol{\mu}_{B0},\; \frac{\lambda_0}{\kappa(\nu_0+1-d)}\Lambda_0\right).$$

Now, let's define $\boldsymbol{\delta} = \boldsymbol{\mu}_A - \boldsymbol{\mu}_B$,

$$\boldsymbol{\delta} \mid \Sigma \;\sim\; \mathcal{N}\left(\delta_0,\; \tfrac{2}{\kappa}\Sigma\right), \delta_0 = \boldsymbol{\mu}_{A0} - \boldsymbol{\mu}_{B0}$$

$$\begin{aligned}
p(\boldsymbol{\delta}) &= \int p(\boldsymbol{\delta} \mid \Sigma)\, p(\Sigma)\, d\Sigma \\
&\propto \int (2\pi)^{-\frac{d}{2}} \left|\tfrac{2}{\kappa}\Sigma\right|^{-\frac{1}{2}} \exp\left(-\tfrac{1}{2}(\boldsymbol{\delta} - \boldsymbol{\delta}_0)^\top \left(\tfrac{2}{\kappa}\Sigma\right)^{-1} (\boldsymbol{\delta} - \boldsymbol{\delta}_0)\right) \\
&\qquad \times \frac{|\lambda_0\Lambda_0|^{\frac{\nu_0}{2}} |\Sigma|^{-\frac{\nu_0+d+1}{2}} \exp\left[-\frac{1}{2}\mathrm{tr}(\lambda_0\Lambda_0\Sigma^{-1})\right]}{2^{\frac{\nu_0 d}{2}} \Gamma_d(\frac{\nu_0}{2})}\, d\Sigma \\
&\propto \frac{2^{\frac{(\nu_0+1)d}{2}} \Gamma\left(\frac{\nu_0+1}{2}\right)}{\left|\lambda_0\Lambda_0 + \frac{\kappa}{2}(\boldsymbol{\delta} - \boldsymbol{\delta}_0)(\boldsymbol{\delta} - \boldsymbol{\delta}_0)^\top\right|^{\frac{\nu_0+1}{2}}} \\
&= \frac{\Gamma\left(\frac{\nu_0+1}{2}\right)}{\Gamma\left(\frac{\nu_0}{2}\right)} \frac{1}{\left[1 + \frac{\kappa}{2\lambda_0}(\boldsymbol{\delta} - \boldsymbol{\delta}_0)^\top \Lambda_0^{-1}(\boldsymbol{\delta} - \boldsymbol{\delta}_0)\right]^{\frac{\nu_0+1}{2}}}.
\end{aligned} \tag{12}$$

Thus,

$$\boldsymbol{\delta} \;\sim\; t_{\nu_0+1-d}\Big(\boldsymbol{\delta}_0,\; \tfrac{2\lambda_0}{\kappa(\nu_0+1-d)}\Lambda_0\Big)\,.$$

Posterior derivation. The posterior distribution is proportional to the product of the likelihood and the prior,

$$p(\boldsymbol{\mu}_A, \boldsymbol{\mu}_B, \Sigma \mid \mathbf{Y}) \;\propto\; L(\boldsymbol{\mu}_A, \boldsymbol{\mu}_B, \Sigma \mid \mathbf{Y}) \times p(\boldsymbol{\mu}_A, \boldsymbol{\mu}_B, \Sigma).$$

For the arm-specific means, the conjugate update implies

$$\boldsymbol{\mu}_A \mid \Sigma, \mathbf{Y} \sim \mathcal{N}\Big(\boldsymbol{\mu}_A^*,\; \frac{1}{\kappa_A^*}\Sigma\Big),$$

where

$$\boldsymbol{\mu}_A^* = \frac{\kappa_{A0}\boldsymbol{\mu}_{A0} + n_A\bar{\mathbf{Y}}_A}{\kappa_{A0} + n_A}, \qquad \kappa_A^* = \kappa_{A0} + n_A,$$

and analogously for arm B.

For the covariance matrix Σ, we first write the likelihood conditional on $\boldsymbol{\mu}_A, \boldsymbol{\mu}_B$ as

$$\begin{aligned}
p(\mathbf{Y}_A, \mathbf{Y}_B \mid \Sigma, \boldsymbol{\mu}_A, \boldsymbol{\mu}_B) \propto{}& \prod_{i=1}^{n_A} |\Sigma|^{-1/2} \exp\Big\{-\frac{1}{2}(\mathbf{Y}_{Ai} - \boldsymbol{\mu}_A)^\top \Sigma^{-1} (\mathbf{Y}_{Ai} - \boldsymbol{\mu}_A)\Big\} \\
&\times \prod_{j=1}^{n_B} |\Sigma|^{-1/2} \exp\Big\{-\frac{1}{2}(\mathbf{Y}_{Bj} - \boldsymbol{\mu}_B)^\top \Sigma^{-1} (\mathbf{Y}_{Bj} - \boldsymbol{\mu}_B)\Big\} \\
\propto{}& |\Sigma|^{-\frac{n_A}{2}} \exp\Bigg(-\frac{1}{2}\sum_{i=1}^{n_A} \mathrm{tr}\big[\Sigma^{-1}(\mathbf{Y}_{Ai} - \boldsymbol{\mu}_A)(\mathbf{Y}_{Ai} - \boldsymbol{\mu}_A)^\top\big]\Bigg) \\
&\times |\Sigma|^{-\frac{n_B}{2}} \exp\Bigg(-\frac{1}{2}\sum_{j=1}^{n_B} \mathrm{tr}\big[\Sigma^{-1}(\mathbf{Y}_{Bj} - \boldsymbol{\mu}_B)(\mathbf{Y}_{Bj} - \boldsymbol{\mu}_B)^\top\big]\Bigg). \qquad (13)
\end{aligned}$$

Define the scatter matrices

$$S_A = \sum_{i=1}^{n_A} (\mathbf{Y}_{Ai} - \boldsymbol{\mu}_A)(\mathbf{Y}_{Ai} - \boldsymbol{\mu}_A)^\top, \qquad S_B = \sum_{j=1}^{n_B} (\mathbf{Y}_{Bj} - \boldsymbol{\mu}_B)(\mathbf{Y}_{Bj} - \boldsymbol{\mu}_B)^\top.$$

Then (13) can be written as

$$\begin{aligned} p(\mathbf{Y}_A, \mathbf{Y}_B \mid \Sigma, \boldsymbol{\mu}_A, \boldsymbol{\mu}_B) &\propto |\Sigma|^{-\frac{n_A}{2}} \exp\left(-\frac{1}{2}\mathrm{tr}\big(\Sigma^{-1} S_A\big)\right) \times |\Sigma|^{-\frac{n_B}{2}} \exp\left(-\frac{1}{2}\mathrm{tr}\big(\Sigma^{-1} S_B\big)\right) \\ &\propto |\Sigma|^{-\frac{n_A+n_B}{2}} \exp\left(-\frac{1}{2}\mathrm{tr}\big[\Sigma^{-1}(S_A + S_B)\big]\right). \end{aligned} \tag{14}$$

The Inverse-Wishart prior is

$$p(\Sigma) \propto |\Sigma|^{-(\nu_0+d+1)/2} \exp\left(-\frac{1}{2}\mathrm{tr}\big(\Lambda\, \Sigma^{-1}\big)\right),$$

where d is the dimension ($d = 2$).

Combining the likelihood (14) and the prior, the conditional posterior of Σ given $\mathbf{Y}_A, \mathbf{Y}_B, \boldsymbol{\mu}_A, \boldsymbol{\mu}_B$ is

$$\begin{aligned} p(\Sigma \mid \mathbf{Y}_A, \mathbf{Y}_B, \boldsymbol{\mu}_A, \boldsymbol{\mu}_B) &\propto |\Sigma|^{-\frac{n_A+n_B}{2}} \exp\left(-\frac{1}{2}\mathrm{tr}\big[\Sigma^{-1}(S_A + S_B)\big]\right) \times |\Sigma|^{-(\nu_0+d+1)/2} \exp\left(-\frac{1}{2}\mathrm{tr}\big(\Lambda\, \Sigma^{-1}\big)\right) \\ &\propto |\Sigma|^{-\frac{\nu_0+n_A+n_B+d+1}{2}} \exp\left(-\frac{1}{2}\mathrm{tr}\big[\Sigma^{-1}(\Lambda + S_A + S_B)\big]\right). \end{aligned} \tag{15}$$

Recognizing this kernel as that of an Inverse-Wishart distribution, we obtain

$$\Sigma \mid \mathbf{Y}_A, \mathbf{Y}_B, \boldsymbol{\mu}_A, \boldsymbol{\mu}_B \sim \mathrm{InvWishart}\big(\nu_0 + n_A + n_B,\ \Lambda + S_A + S_B\big).$$

$$\mathbb{E}[\Sigma \mid D_A, D_B] = \frac{S_A + S_B + \Lambda}{n_A + n_B + \nu_0 - d - 1} \tag{16}$$

7.2 Insensitivity to prior correlation

The prior correlation ρ_0 enters the posterior of Σ only through the scale matrix $\Lambda + S_A + S_B$, where $\Lambda = \lambda_0 \Lambda_0$. We show that under the default $\nu_0 = 2$, the contribution of ρ_0 to the posterior is negligible.

Proof. By linearity of the trace, from Equation 15,

$$\mathrm{tr}\left[\Sigma^{-1}(\Lambda + S_A + S_B)\right] = \mathrm{tr}\left[\Sigma^{-1}\lambda_0\Lambda_0\right] + \mathrm{tr}\left[\Sigma^{-1}(S_A + S_B)\right].$$

Evaluate the first term. With $\sigma_1 = \sigma_2 = 1$,

$$\Sigma^{-1} = \frac{1}{1-\rho^2}\begin{pmatrix} 1 & -\rho \\ -\rho & 1 \end{pmatrix}, \qquad \Lambda_0 = \begin{pmatrix} 1 & \rho_0 \\ \rho_0 & 1 \end{pmatrix}.$$

Then,

$$\Sigma^{-1}\lambda_0\Lambda_0 = \frac{\lambda_0}{1-\rho^2}\begin{pmatrix} 1 & -\rho \\ -\rho & 1 \end{pmatrix}\begin{pmatrix} 1 & \rho_0 \\ \rho_0 & 1 \end{pmatrix} = \frac{\lambda_0}{1-\rho^2}\begin{pmatrix} 1-\rho\rho_0 & \rho_0 - \rho \\ -\rho + \rho_0 & 1-\rho\rho_0 \end{pmatrix}.$$

Taking the trace,

$$\mathrm{tr}\left[\Sigma^{-1}\lambda_0\Lambda_0\right] = \frac{2\lambda_0(1-\rho\,\rho_0)}{1-\rho^2}.$$

The second term $\mathrm{tr}[\Sigma^{-1}(S_A + S_B)]$ depends only on the data through the scatter matrices and contains no prior hyperparameters. Therefore, ρ_0 can only influence the posterior through

the first term $\mathrm{tr}[\Sigma^{-1}\lambda_0\Lambda_0]$.

The change in the prior trace contribution when ρ_0 shifts from 0 to some value ρ_0' is

$$\Delta_{\rho_0} = \left|\frac{2\lambda_0(1-\rho\,\rho_0')}{1-\rho^2} - \frac{2\lambda_0}{1-\rho^2}\right| = \frac{2\lambda_0\,|\rho|\,|\rho_0'|}{1-\rho^2}.$$

For the second term, with $S_A + S_B \approx (n_A + n_B)\hat{\Sigma}$ where $\hat{\Sigma} \approx \Sigma$,

$$\mathrm{tr}\big[\Sigma^{-1}(S_A + S_B)\big] \approx (n_A + n_B)\,\mathrm{tr}(I_d) = d(n_A + n_B).$$

The ratio of the ρ_0-induced change to the data contribution is therefore

$$\frac{\Delta_{\rho_0}}{d(n_A + n_B)} = \frac{2\lambda_0\,|\rho|\,|\rho_0'|}{(1-\rho^2)\,d(n_A + n_B)} = O\left(\frac{\lambda_0}{n}\right). \tag{17}$$

Under the default $\nu_0 = 2$, the calibrated λ_0 is small (e.g., $\lambda_0 = 0.02$ at $\kappa = 1$, and $\lambda_0 = 0.194$ at $\kappa = 10$).

Thus, even at the smallest sample size considered ($n = 10$ per arm) and the largest prior precision ($\kappa = 10$), the ratio remains below 1% for moderate correlations ($|\rho| \leq 0.6$). The factor $1/(1-\rho^2)$ in the prior trace term means that very high true correlations ($|\rho| > 0.9$) could amplify the prior's contribution, but the ratio remains bounded by $O(\lambda_0/n)$ and does not exceed 3% even at $|\rho| = 0.9$ under the default $\nu_0 = 2$. Crucially, ρ_0 enters only in the numerator through $|\rho_0'| \leq 1$, so changing ρ_0 from 0 to any value in $(-1, 1)$ cannot increase the order of the ratio beyond $O(\lambda_0/n)$. □

7.3 Proposition proof

Lemma 1 (Continuity)**.** *For fixed $\nu_0 > d - 1$, $\kappa > 0$, and $\boldsymbol{\delta}_0 \neq \boldsymbol{\tau}$, $f(\lambda_0)$ is continuous in λ_0 on $(0, \infty)$.*

Proof. Each component of $\mathbf{z}(\lambda_0)$ is proportional to $\lambda_0^{-1/2}$, which is continuous on $(0, \infty)$.

The bivariate t survival function $\bar{F}_{\nu_0+1-d}(\mathbf{z}; R)$ is continuous in $\mathbf{z}$ because it is defined by integration of a continuous density over a region whose boundary moves continuously with $\mathbf{z}$. The composition of continuous functions is continuous. □

Lemma 2 (Monotonicity)**.** *Under the same conditions, $f(\lambda_0)$ is strictly monotone in λ_0 on $(0, \infty)$.*

Proof. As λ_0 increases, each component of $\mathbf{z}(\lambda_0)$ moves toward zero, since $|z_j(\lambda_0)| \propto \lambda_0^{-1/2}$. For the skeptical prior, $\boldsymbol{\delta}_0$ lies below $\boldsymbol{\tau}$ componentwise, so $\boldsymbol{\tau} - \boldsymbol{\delta}_0 > \mathbf{0}$ and $\mathbf{z}(\lambda_0) > \mathbf{0}$. As λ_0 increases, $\mathbf{z}(\lambda_0)$ decreases toward $\mathbf{0}$, and the upper orthant probability $\bar{F}_{\nu_0+1-d}(\mathbf{z}; R)$ increases (since less of the distribution is excluded). Hence f is strictly increasing in λ_0.

For the enthusiastic prior, $\boldsymbol{\delta}_0$ lies above $\boldsymbol{\tau}$, so by the analogous argument applied to the lower orthant, f is also strictly increasing in λ_0.

In both cases, the strict monotonicity follows from the fact that the bivariate t density is strictly positive everywhere, so any shift in $\mathbf{z}$ produces a strict change in the orthant probability.

□

Lemma 3 (Boundary limits)**.** *Under the same conditions,*

$$\lim_{\lambda_0 \to 0} f(\lambda_0) = 0, \qquad \lim_{\lambda_0 \to \infty} f(\lambda_0) = L,$$

where $L = P(T_1 > 0, T_2 > 0)$ is the positive orthant probability of a centered bivariate t distribution with correlation matrix Λ_0 and $\nu_0 + 1 - d$ degrees of freedom.

Proof. (i) As $\lambda_0 \to 0$: each component of $\mathbf{z}(\lambda_0)$ diverges to $+\infty$ (skeptical case) or $-\infty$ (enthusiastic case). In the skeptical case, the upper orthant probability $P(\mathbf{T} > \mathbf{z})$ vanishes as $\mathbf{z} \to +\infty$. In the enthusiastic case, the lower orthant probability $P(\mathbf{T} < \mathbf{z})$ vanishes as $\mathbf{z} \to -\infty$. Hence $f(\lambda_0) \to 0$ in both cases.

(ii) As $\lambda_0 \to \infty$: $\mathbf{z}(\lambda_0) \to \mathbf{0}$, so

$$f(\lambda_0) \to P(\mathbf{T} > \mathbf{0}) = P(T_1 > 0,\, T_2 > 0) = L.$$

When $\rho_0 = 0$, the bivariate t orthant probability equals $1/4$ by symmetry. More generally, for large ν_0 the t distribution is well approximated by a bivariate normal, yielding [21]

$$L \approx \frac{1}{4} + \frac{1}{2\pi} \arcsin(\rho_0).$$

Since $L \in (0, 1)$ and f is continuous and strictly increasing from 0 to L, the intermediate value theorem guarantees a unique $\lambda_0^* > 0$ satisfying $f(\lambda_0^*) = \alpha$ for any $\alpha \in (0, L)$. □

Proof of Proposition 1. Lemma 1 establishes that $f(\lambda_0)$ is continuous on $(0, \infty)$, Lemma 2 that it is strictly monotone, and Lemma 3 that it maps onto $(0, L)$. By the intermediate value theorem, every $\alpha \in (0, L)$ is attained, and strict monotonicity guarantees the solution λ_0^* is unique. Since these properties hold for any fixed $\kappa > 0$, the existence and uniqueness of $\lambda_0^*(\kappa)$ extends to all κ. □ □

7.4 TABLES

Table S1: Prior specifications for the eight prior distributions. For each prior, λ_0 is calibrated via calibration function where the tail probability at the specified threshold equals the target probability, reported separately for each value of ν_0. All priors use $\kappa_{A0} = \kappa_{B0} = 1$ and $\rho_0 = 0$.

Prior	Center	Threshold	Target Prob.	Region	λ_0			
					$\nu_0 = 2$	$\nu_0 = 4$	$\nu_0 = 10$	$\nu_0 = 50$
Skeptical priors								
Skeptical	(0.0, 0.0)	(0.5, 0.5)	0.05	Upper	0.02	0.2	0.84	5.16
Extreme skeptical	(0.0, 0.0)	(0.5, 0.5)	0.01	Upper	0.01	0.04	0.26	1.77
Extreme skeptical v2	(−1.0, −1.0)	(−0.5, −0.5)	0.05	Upper	0.02	0.2	0.84	5.16
Extreme skeptical v3	(−1.0, −1.0)	(−0.5, −0.5)	0.01	Upper	0.01	0.04	0.26	1.77
Enthusiastic priors								
Enthusiastic	(0.5, 0.5)	(0.0, 0.0)	0.05	Lower	0.02	0.2	0.84	5.16
Extreme enthusiastic	(0.5, 0.5)	(0.0, 0.0)	0.01	Lower	0.01	0.04	0.26	1.77
Extreme enthusiastic v2	(1.5, 1.5)	(1.0, 1.0)	0.05	Lower	0.02	0.2	0.84	5.16
Extreme enthusiastic v3	(1.5, 1.5)	(1.0, 1.0)	0.01	Lower	0.01	0.04	0.26	1.77

Prior center denotes the location parameter (δ_1, δ_2) of the marginal multivariate t prior on the treatment effect $\delta = \mu_A - \mu_B$. Threshold denotes the boundary at which the tail probability is calibrated. Upper tail: $P(\delta > \text{threshold}) = \text{target prob.}$; Lower tail: $P(\delta < \text{threshold}) = \text{target prob.}$

Table S2: Operating characteristics of the Bayesian Go/No-Go decision rule under the both-effects scenario with $n = 10$ per arm, $\rho_0 = 0$, $\rho_{\text{true}} = 0$, and 10,000 simulation replications. Three true effect sizes are considered: null ($\boldsymbol{\delta} = \mathbf{0}$), moderate ($\boldsymbol{\delta} = 0.5$), and strong ($\boldsymbol{\delta} = 1$), where $\boldsymbol{\delta} = (\delta_1, \delta_2)$. Go rate is the proportion of simulations in which $P(\delta_1 > 0, \delta_2 > 0 \mid \text{data}) > 0.95$. Under the null scenario, go rate corresponds to the empirical false positive rate. Prior specifications are detailed in Table 2.

		Go Rate			Avg. Posterior Prob.		
ν_0	Prior	Null	Moderate	Strong	Null	Moderate	Strong
2	Skeptical	0.0021	0.0658	0.4417	0.2502	0.6244	0.8835
	Enthusiastic	0.0027	0.0902	0.5097	0.2848	0.6609	0.9018
4	Skeptical	0.0024	0.0801	0.4824	0.2502	0.6320	0.8910
	Enthusiastic	0.0042	0.1081	0.5487	0.2854	0.6689	0.9086
10	Skeptical	0.0048	0.1193	0.5692	0.2503	0.6495	0.9071
	Enthusiastic	0.0076	0.1541	0.6304	0.2869	0.6872	0.9232
50	Skeptical	0.0223	0.2806	0.7764	0.2506	0.6970	0.9428
	Enthusiastic	0.0305	0.3333	0.8145	0.2911	0.7360	0.9546

For each ν_0, λ_0 is uniquely determined by the calibration function (Proposition 1). All priors use $\kappa_{A0} = \kappa_{B0} = 1$.

Table S3: Go rates for skeptical and enthusiastic priors across $\kappa \in \{1, 5, 10\}$ and sample sizes, under the both-effects scenario, $\nu_0 = 2$, $\rho_0 = 0.6$, $c = 0.95$, 10,000 replications. For each κ, λ_0 is recalibrated to maintain the target tail probability of 0.05.

		$\rho_0 = 0.6,\ \rho_{\text{true}} = 0$			$\rho_0 = 0.6,\ \rho_{\text{true}} = 0.6$		
κ	Prior	Null	Mod.	Strong	Null	Mod.	Strong
$n = 10$ *per arm*							
1	Skeptical	0.0012	0.0696	0.4548	0.0141	0.1418	0.5327
	Enthusiastic	0.0018	0.0937	0.5229	0.0185	0.1755	0.5939
5	Skeptical	0.0001	0.0224	0.2347	0.0050	0.0674	0.3404
	Enthusiastic	0.0035	0.1197	0.5674	0.0253	0.2111	0.6310
10	Skeptical	0.0000	0.0032	0.0696	0.0013	0.0252	0.1609
	Enthusiastic	0.0078	0.1786	0.6491	0.0412	0.2837	0.6957
$n = 25$ *per arm*							
1	Skeptical	0.0011	0.2577	0.9315	0.0129	0.3654	0.9397
	Enthusiastic	0.0017	0.2920	0.9414	0.0153	0.3982	0.9480
5	Skeptical	0.0005	0.1958	0.8987	0.0087	0.3034	0.9131
	Enthusiastic	0.0029	0.3534	0.9580	0.0244	0.4604	0.9631
10	Skeptical	0.0001	0.1334	0.8471	0.0050	0.2368	0.8668
	Enthusiastic	0.0056	0.4470	0.9736	0.0360	0.5409	0.9763
$n = 50$ *per arm*							
1	Skeptical	0.0011	0.6152	0.9988	0.0119	0.6718	0.9995
	Enthusiastic	0.0019	0.6377	0.9991	0.0136	0.6907	0.9995
5	Skeptical	0.0006	0.5793	0.9987	0.0093	0.6411	0.9989
	Enthusiastic	0.0033	0.6984	0.9997	0.0191	0.7394	0.9996
10	Skeptical	0.0004	0.5309	0.9982	0.0070	0.6049	0.9983
	Enthusiastic	0.0056	0.7659	0.9998	0.0284	0.7893	0.9998

ρ_0: prior correlation in Λ_0; ρ_{true}: true correlation used to generate data. Null: $\boldsymbol{\delta} = (0, 0)$; Moderate (Mod.): $\boldsymbol{\delta} = (0.5, 0.5)$; Strong: $\boldsymbol{\delta} = (1, 1)$.

7.5 Figures

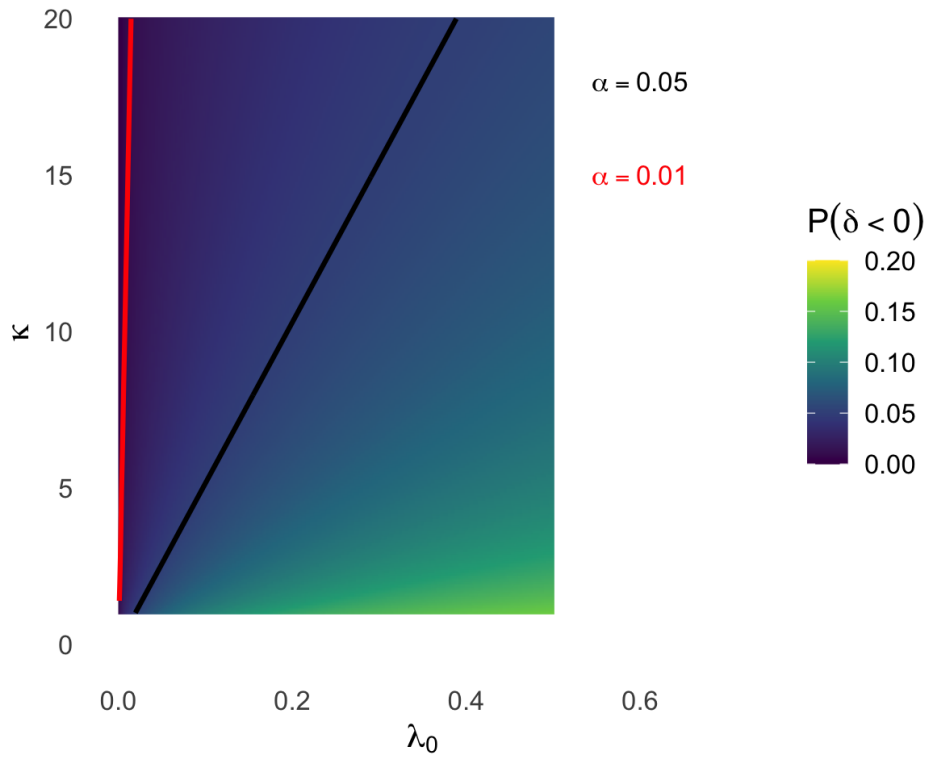

(a) $\rho_0 = 0$

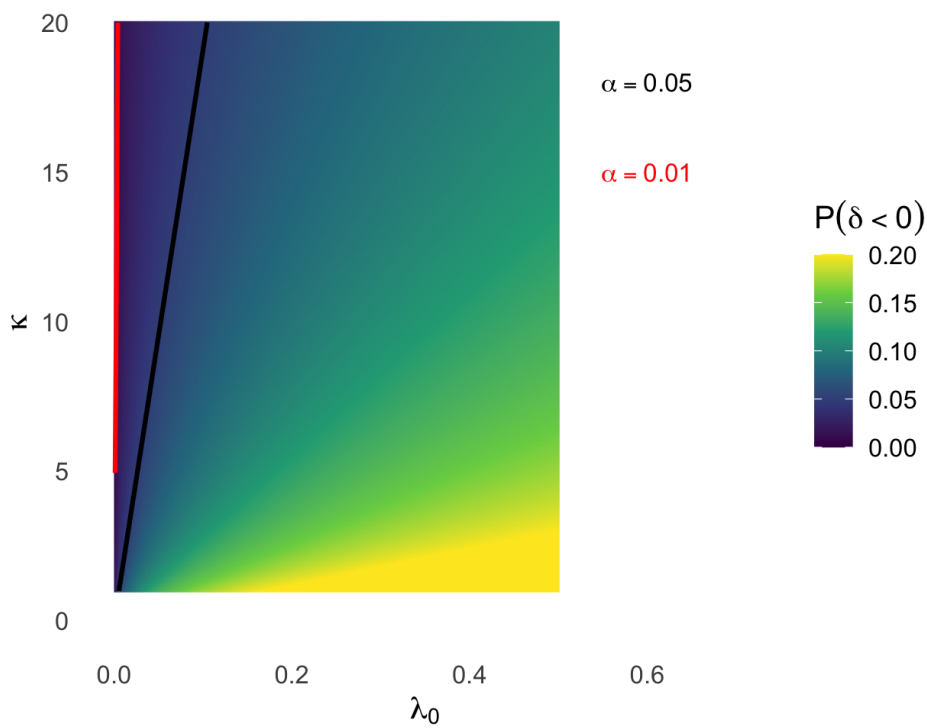

(b) $\rho_0 = 0.6$

Figure S1: Calibration function $P(\boldsymbol{\delta} > \boldsymbol{\tau})$ for the enthusiastic prior across (κ, λ_0) with $\nu_0 = 2$. Contour lines indicate $\alpha = 0.05$ (black) and $\alpha = 0.01$ (red). The contour lines trace the (κ, λ_0) pairs satisfying the calibration in Proposition 1.